PCCP

ROYAL SOCIETY OF CHEMISTRY

PAPER

View Article Online
View Journal | View Issue



Cite this: *Phys. Chem. Chem. Phys.*, 2023, **25**, 2153

# A direct approach toward investigating DNA–ligand interactions *via* surface-enhanced Raman spectroscopy combined with molecular dynamics simulations†

Yunpeng Wang, ‡[b] Na Shi,‡[a] Yingying He,[b] Yang Li *[b] and Qingchuan Zheng *[a]

Small molecules that interfere with DNA replication can trigger genomic instability, which makes these molecules valuable in the search for anticancer drugs. Thus, interactions between DNA and its ligands at the molecular level are of great significance. In the present study, a new method based on surface-enhanced Raman spectroscopy (SERS) combined with molecular dynamics simulations has been proposed for analyzing the interactions between DNA and its ligands. The SERS signals of DNA hairpins (ST: d(CGACCAACGTGTCGCCTGGTCG), AP1: d(CGCACAACGTGTCGCCTGTGCG)), pure argininamide, and their complexes, were obtained, and the characteristic peak sites of the DNA secondary structure and argininamide ligand-binding region were analyzed. Molecular dynamics calculations predicted that argininamide binds to the 8C and 9G bases of AP1 *via* hydrogen bonding. Our method successfully detected the changes of SERS fingerprint peaks of hydrogen bonds and bases between argininamide and DNA hairpin bases, and their binding sites and action modes were consistent with the predicted results of the molecular dynamics simulations. This SERS technology combined with the molecular dynamics simulation detection platform provides a general analysis tool, with the advantage of effective, rapid, and sensitive detection. This platform can obtain sufficient molecular level conformational information to provide avenues for rapid drug screening and promote progress in several fields, including targeted drug design.

Received 30th September 2022,
Accepted 4th December 2022

DOI: 10.1039/d2cp04566d

rsc.li/pccp



## Introduction

Genomic DNA contains local and temporary tertiary structures that hinder its replication process.[1,2] Small molecules that promote and/or stabilize higher-order DNA folding are promising targets as cytotoxic agents. Owing to their potential in treating cancer efficiently, small molecules have attracted significant research interest.[3] For example, argininamide analogs have important implications for the transactivation response region (TAR) RNA bonding.[4–6] Among them, the hairpin aptamer TAR RNA in HIV-1 RNA specifically recognizes arginine in HIV's transcriptional transactivator, a key step in HIV gene expression.[7,8] However, the exact manner in which these ligands bind to their associated DNA sequence remains unclear and is under investigation. Therefore, there is an urgent need to develop efficient and reliable bioassays for monitoring and quantifying interactions between DNA and its ligands.

Previous studies employed nuclear magnetic resonance spectroscopy,[9–11] X-ray diffraction,[12,13] and molecular simulation[14–16] to obtain the structural parameters of DNA and its ligands at the molecular level, providing an improved understanding of the interactions between DNA and its ligands. However, the excessive sample concentration in nuclear magnetic resonance spectroscopy and the complicated crystallization process in X-ray diffraction not only affect the true DNA structure but also greatly increase the detection cost. This limits the general application of these methods in resolving interactions between DNA and its ligands. Other relatively simple methods for sample preparation, including UV-vis absorption spectroscopy, fluorescence spectroscopy, and circular dichroism (CD) have also been used to study changes in the DNA structure after ligand binding.[17–19] These techniques can easily obtain ligand binding affinity and DNA conformation information; however, these techniques can only obtain macroscopic

[a] *Institute of Theoretical Chemistry, College of Chemistry, Jilin University, Changchun, 130023, China. E-mail: zhengqc@jlu.edu.cn*
[b] *College of Pharmacy, Research Center for Innovative Technology of Pharmaceutical Analysis, Harbin Medical University, Harbin, Heilongjiang, 150081, China. E-mail: liy@hrbmu.edu.cn*

† Electronic supplementary information (ESI) available. See DOI: https://doi.org/10.1039/d2cp04566d

‡ These authors contributed equally to this work.

conformational changes after DNA–ligand binding, whereas subtle structural changes after DNA–ligand binding cannot be deciphered. Other analytical methods, such as thermal melting analysis, isothermal titration calorimetry, and surface plasmon resonance spectroscopy, are also used to determine the thermodynamic and kinetic parameters of the interactions between DNA and its ligands.[20,21] However, these technologies employ integrated analysis, which lack sensitivity and make detecting changes in the DNA structure at the molecular level difficult. Single-molecule fluorescence resonance energy transfer spectroscopy and optical tweezers have also been used for studying DNA–ligand interactions in addition to the kinetic conformation and mechanical information.[22] These methods, however, despite their high sensitivity, require time-consuming, expensive fluorescence labeling and chemical modification processes. Therefore, more efficient and reliable biophysical techniques are needed for exploring the interaction of the DNA structure and its ligands.

Surface-enhanced Raman spectroscopy (SERS) is an effective tool for detecting biomolecules (DNA, RNA, or proteins). The technique is quick, highly sensitive, and requires fewer samples.[23–27] Unlike the abovementioned traditional DNA detection methods, Raman spectroscopy can provide unique structural information at the level of small molecules or lower. This unique structural information is generated by molecular vibrations in a specific conformation. Bell *et al.*[28] successfully used hydroxylamine to reduce the silver colloid to obtain the SERS spectra of short-sequence nucleic acids with good reproducibility. In short-sequence nucleic acids, the single-base mismatches in the ssDNA sequence of 23 nucleotides were identified; however, the surface of the hydroxylamine-reduced silver colloid has a positive charge, which affects the nucleic acid structure. Subsequently, Ren *et al.*[23,29] post-processed the reduction of citrate to silver nanoparticles using iodide ions to modify the surface of the nanoparticles and remove citrate ions and random surface impurities. The content of bases in the ssDNA structure was quantitatively analyzed, and the application of the iodide ion made it possible to maintain the natural structure of the nucleic acid during SERS detection. Wei *et al.*[30] used the SERS indirect method to obtain the SERS spectra of H2TMPyP4 before and after mixing with three different G-quadruples and proposed the interaction model between H2TMPyP4 and a single *G*-quadruple based on the SERS spectral changes of H2TMPyP4 (non-*G*-quadruples). Unfortunately, the SERS signal of the DNA molecule itself was not obtained. At present, in the literature, the method of using SERS to directly detect DNA and its ligands has not been reported. This is because owing to the relatively rigid high-level structure of DNA, it is difficult to detect the inherent SERS signal compared with that of the single-strand structure of DNA, thereby greatly limiting the application of SERS for detecting the DNA molecular structure.[31] Therefore, in the present study, SERS was used to directly analyze the interaction data between DNA molecules without any modification or labeling and their small molecule ligands so that SERS can be used as an effective means to study biomolecules and their ligand complexes.

In the present study, SERS was used for the first time to trace changes in the DNA structure due to the interaction of the argininamide ligand with specific DNA sequences (Fig. 1, specific experimental scheme). Through the characteristic peak changes in hydrogen bonds and bases, the corresponding SERS fingerprint bands before and after DNA binding with ligand were determined, which confirmed the noncovalent bond interaction between the argininamide ligand and the specific DNA hairpin bases. The prediction of binding sites and modes of action based on the molecular dynamics simulation was consistent with the conclusion of the current method confirming the accuracy of our method. In this work, a new platform was established for studying the interactions between DNA and its ligands.

## Experimental

### Preparation of silver nanoparticles

Silver nanoparticles with citrate ions on the surface were prepared according to the Lee method.[32] In brief, 0.07 g of silver nitrate and 400 mL of deionized water were added to a three-neck flask and heated to near-boiling temperature under constant stirring. Then, 12 mL of 1% sodium citrate solution was added, and the solution was cooled to room temperature to obtain the silver nanoparticle product (Ag@cit). Then, 50 μL of Ag@cit were centrifuged at 5000 rpm for 15 min, the

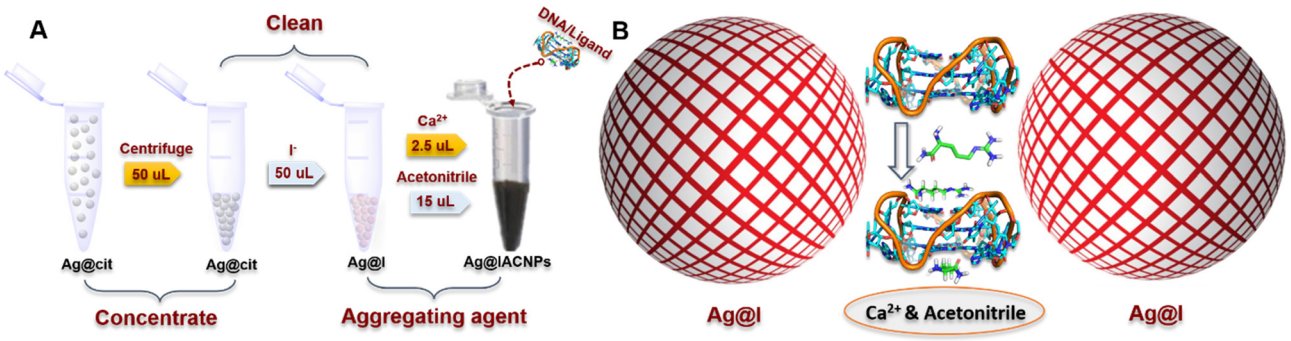


Fig. 1 Schematic diagram of the experimental process; (A) The procedure of the "hot spot" formed by iodide ion modified silver nanoparticles; (B) Schematic diagram of DNA and its ligand complex in the "hot spot" which induced by calcium ion.

 

supernatant was removed, 50 μL of 1 mM KI was added, and the product (Ag@I) was incubated overnight and stored in the dark.

### Preparation of DNA samples

DNA (high-performance liquid chromatography grade) used in this study was purchased from Sangon Biotech (Shanghai) Co., Ltd. Ultrapure water was added to the lyophilized DNA to prepare a 1 mM DNA stock solution and stored at −20 °C. Then, 10 μL of DNA stock solution [ST d(CGACCAACGT-GTCGCCTGGTCG) AP1 d(CGCACAACGTGTCGCCTGTGCG)] was added to 10 μL of ammonium acetate buffer solution (pH = 4.5; 500 mM) and 80 μL of water. The solution was heated in a water bath at 90 °C for 10 min, until the water bath cooled naturally, and the solution was stored at 4 °C for 5 days after incubating for 12 h at room temperature. The product was characterized using CD. As shown in Fig. S1 (ESI†), the CD results indicated that the DNA hairpin structure was completely synthesized, consistent with published literature.[31,33,34] DNA hairpin products (ST and AP1) were incubated with equal volumes of argininamide ligands (2, 4, and 6 mM) for 4 days to form DNA–argininamide complexes (STA and APA).

### CD spectroscopy

CD spectral data were obtained using a CS30152 instrument (Applied PhotoPhysics, Surrey, UK). A sample pool of 0.5 mm path length was used, with the wavelength range of 320–200 nm, and scanning was performed three times to calculate the average spectrogram at a scan speed of 100 nm $min^{-1}$, 0.5 s per point, 1 nm bandwidth, and 1 nm data interval. The final DNA concentration for CD detection was 12.5 μM, and the background spectrum of buffer was subtracted from the obtained DNA spectrum.

### SERS spectral detection

Approximately 10 μL of silver nanoparticles (Ag@I) were added to a 1.5 mL centrifuge tube. Then, 50 μL of STA sample, 15 μL of acetonitrile, and 2.5 μL of calcium solution were added to the centrifuge tube. The components were mixed and shaken well, and a small amount of the mixed sample was absorbed using a 0.5 mm capillary tube for SERS detection. The instrument used in the Raman experiment was WITec alpha300 RA (Germany). The instrument parameters are as follows: laser wavelength: 633 nm; grating: 600; resolution: 3 $cm^{-1}$; scanning time: 60 s per time; laser power: 10 mW; and cumulative scanning time: 1 time. All Raman spectroscopy signal data presented in this study do not include any other smoothing operation except the base operation.

### Theoretical calculation methods

**Model preparation and molecular docking.** In order to construct the three-dimensional structure of the DNA hairpin structure of AP1,the crystal structure (PDB ID: 1DB6)[35] from the Protein Data Bank that is very close to the AP1 sequences was selected as a template. 3A, 4C, 19G and 20T in 1DB6 were modified to 3C, 4A, 19T and 20G by means of the Discovery Studio 3.1 software.[36] The modified three-dimensional structure was first optimized by AMBER 16 software,[37] and the duration of the molecular dynamics simulations is 100 ns. The optimized structure was used as the receptor for molecular docking. The argininamide molecule was optimized by Gaussian 09 software at B3lYP/6-31G(d).[38,39] The CDOCKER module of Discovery Studio 3.1 software[36] was used for molecular docking. The conformation with the highest score was determined as the most optimum structure (APA complex) for the next molecular dynamics simulations.

**Molecular dynamics simulations.** The charge distributions of argininamide were measured using the RESP (restrained electrostatic potential)[40] and the force field parameters were obtained through the Antechamber module.[41] The force fields of DNA and argininamide are described by ff14SB[42] and GAFF.[43] The hydrogen atoms and counterbalance ions were added to the system by the *tleap* module.[37] The system was immersed in a TIP3P water box,[44] and the minimum distance between the water box boundary and the protein boundary atom is 10 Å. The solutes (DNA and argininamide) were fixed with a force of 500 $kcal^{-1}$ $mol^{-1}$ $Å^{-2}$. The solvent was minimized by 10 000 steps of the steepest descent followed by 10 000 steps of conjugate gradient on the solvent. Then, the solute was released from the restriction and the steepest descent and conjugate gradient with the same number of steps were used to remove the bad contacts in the system. The system was gradually heated from 0 K to 300 K in 1000 ps under the *NVT* ensemble. After heating, the system was subjected to a 1000 ps equilibrium. To maintain the stability of the system in the process of heating and equilibrium, the skeleton atoms of the system were restricted by 5 $kcal^{-1}$ $mol^{-1}$ $Å^{-2}$. Finally, 100 ns molecular dynamics simulations were performed in the *NPT* ensemble. During the molecular dynamics simulations, the Particle Mesh Ewald (PME)[45] method deals with long-range electrostatic interactions. The cutoff value for short-range interactions is 10 Å. The SHAKE algorithm[46] is applied to the chemical bonds containing hydrogen atoms in the system. The *cpptraj* module[37] was used for the root mean square deviation (RMSD, Fig. S2, ESI†) and hydrogen bond interaction analysis (Fig. 5C).

## Results and discussion

The main challenge of using SERS to detect DNA structures without labels is the difficulty in obtaining clear and repeatable SERS signals. After coordinating with small molecule ligands, it is actually more difficult to detect SERS signals owing to the rigid DNA structure. Fig. 2A illustrates that the sodium citrate-reduced silver nanoparticles (Ag@cit) have a Raman signal (blue line) and that the DNA samples to be tested are easily disturbed by the citrate signal and cannot be identified. To avoid the interference of the citrate signal, iodide ions were introduced to replace the citrate root on the surface of the nanoparticles; the obtained silver nanoparticles (Ag@I) had almost no SERS signal (green line). In the UV-vis absorption spectrum, the local surface plasmon resonance band of Ag@cit was observed at 407 nm; however, after iodide incubation Ag@I

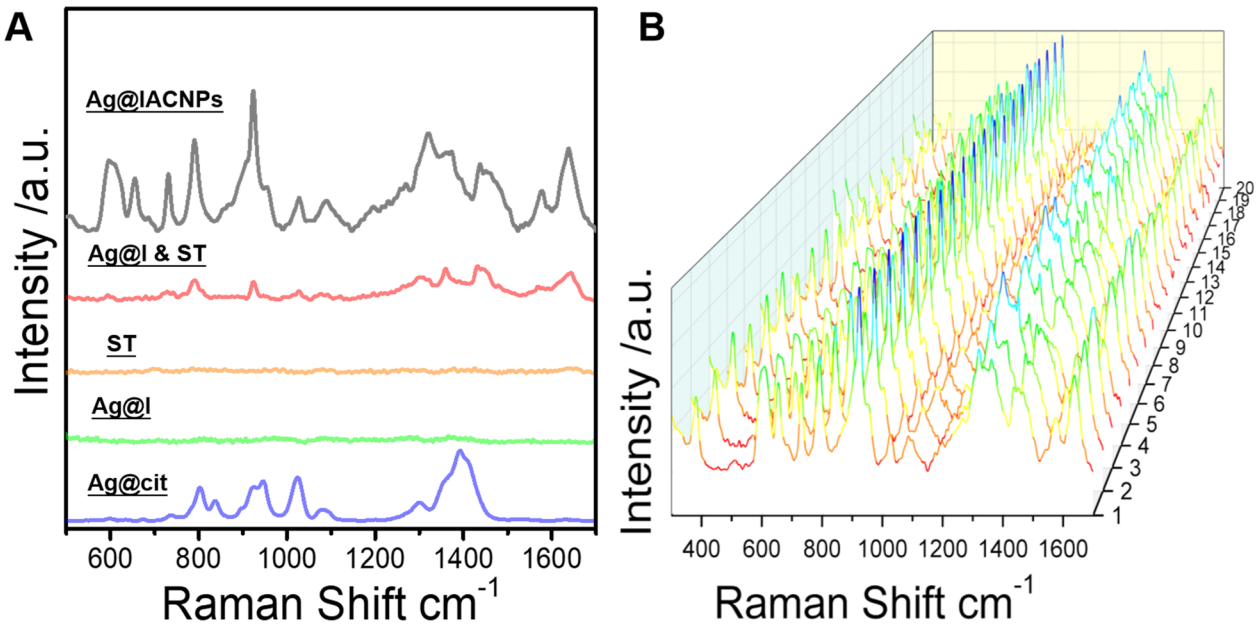


Fig. 2 (A) SERS spectrum of silver nanoparticles (Ag@cit) (blue line); SERS spectrum of silver nanoparticles (Ag@I) after incubation (green line); SERS spectrum of the ST sample in the ammonium acetate buffer solution (pH = 4.5; 500 mM) (orange line); SERS spectrum of the ST samples in the ammonium acetate buffer solution (pH = 4.5; 500 mM) obtained(Ag@I) (red line); and SERS spectrum of the STA sample using the current method (Ag@IACNPs: Ag@I with acetonitrile and calcium ions added) (gray line). (B) SERS spectra obtained from 20 sets of random STA complexes using the current method (Ag@IACNPs).

showed a blue shift to 405 nm (Fig. S3, ESI†). Combined with dynamic light scattering (DLS) analysis, the Ag@cit nanoparticles had two stable states. The average diameter of the silver nanoparticles (Ag@cit) was 10.75 and 79.08 nm, respectively, for the two stable states. The average zeta potential of Ag@cit was −15.2 mV. The silver nanoparticles (Ag@I) and their clusters were 9.8 and 74.11 nm after iodide modification, respectively. The mean zeta potential of Ag@cit was −17.6 mV (Fig. S4, ESI†). Transmission electron microscopy revealed that the silver nanoparticles were predominantly spherical in nature,[47] and the particle size is consistent with the DLS results (Fig. S5, ESI†). The above experimental results showed that the radius of silver nanoparticles decreases with the replacement of citrate by iodide ions, generating a powerful condition for generating more ''hot spot''. DNA biomolecules had no Raman signal, but ST samples in the ammonium acetate solution (pH = 4.5; 500 mM) with Ag@I nanoparticles produced a weak but clear SERS signal (red line). According to the SERS surface selection rules,[48–51] ST molecules may ''stand'' on the surface of silver nanoparticles in ''hot spot'' and ST molecules perpendicular to the matrix surface increase the Raman cross section and enhance the Raman signal. The current method (Ag@IACNPs: silver nanoparticles modified by iodide ions and added with acetonitrile and calcium ions) introduced a calcium ion aggregator and acetonitrile internal standard to significantly enhance the SERS signal of DNA and ligand in STA (gray line). To obtain high quality DNA signals, we selected the calcium ion as the aggregator because it can form a stable complex with citrate, which consequently avoids the influence of interference signals.[52] At the same time, a large number of ''hot spots'' were formed through the calcium ion guided Ag@I aggregation, which significantly enhanced the Raman signal of the target molecules. In addition, because acetonitrile is miscible with water, it can be evenly dispersed in the system, and acetonitrile has clear and stable characteristic peaks (Fig. S6, ESI†), which can be used as an internal standard. Fig. 2B illustrates the random SERS spectra of 20 STA at different time intervals (the above spectra are from four different experiments; each experimental sample was detected five times). The results showed that the current method was beneficial for obtaining a clear and stable SERS signal of the DNA–ligand complex.

To validate the approach for detecting DNA–ligand complexes, the SERS spectra of STA complexes with different proportions were demonstrated. Acetonitrile was used as the internal standard (characteristic peak: 381 $cm^{-1}$) and then normalized. In addition, the CD spectra were compared before and after adding acetonitrile molecules to STA. Almost no change in the CD spectra was observed before and after the addition of acetonitrile molecules, indicating that the configuration of DNA hairpin samples was unaffected by the presence of trace acetonitrile molecules (Fig. S7, ESI†).

In Fig. 3, the SERS signals of the STA complex can be clearly observed (argininamide, amide: 615 $cm^{-1}$ and CN: 924 $cm^{-1}$ and ST, adenine: 731 $cm^{-1}$; cytosine: 791 $cm^{-1}$: guanine: 654, 956, and 1575 $cm^{-1}$; and thymine: 1638 $cm^{-1}$). The detailed peak position attribution is shown in Table S1 (ESI†). The CD data showed a positive band near 284 nm and a negative band near 242 nm (Fig. S8A, ESI†), and the peaks at 284 and 242 nm were associated with the ring structure, suggesting that STA interacts with the ligand and does not modify its DNA hairpin

 

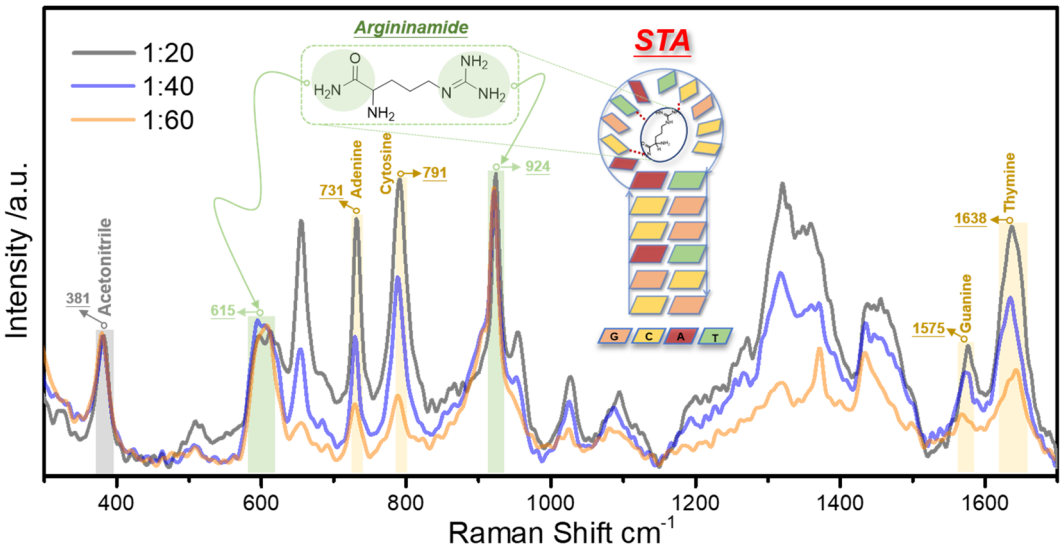


Fig. 3 SERS spectra of the STA complex at different proportions (ST: argininamide = 1 : 20; 1 : 40; and 1 : 60).

configuration. Of note, the amount of acetonitrile and ST was constant, whereas the mass of argininamide gradually increased, and the intensity of argininamide characteristic peak was almost constant. Because under the conditions of different proportions, the amount of ST was constant, the amount of argininamide bonded with it was also constant. So current method could only detect small molecule ligands bonded to DNA. To verify the above conclusion, the Raman signals of T12 sequence (d(TTTTTTTTTTTTTT)), pure argininamide and its incubation were detected. Argininamide does not bind to T12 easily because of its complex structure. So, only the signal of pure argininamide and T12 sequence was observed and the Raman signal of argininamide after incubation was not detected (Fig. S9, ESI†). The results showed that when the current method detects low argininamide concentration, the Raman signal can be detected only when argininamide produces bonds with DNA, and the noncovalent bond interaction between DNA and argininamide is further verified.

Fig. 4 illustrates the SERS characteristic peaks of the pure argininamide ligand (orange line), ST (gray line) and STA (blue line). After the formation of the STA complex, the characteristic signs of C, $C^+$, and $C{\cdot}C^+$ protonation appeared at 1196, 1256, 1269, and 1407 $cm^{-1}$. After protonation, the deoxyribose ring respiration of the cytosine marker was detected at 791 $cm^{-1}$, with the migration at 791–790 $cm^{-1}$ (blue line, assigned to C, $C^+$, and $C{\cdot}C^+$). The results showed that there was bond cooperation between argininamide and the C base of ST after incubation. The two characteristic peaks of STA at 596 and 924 $cm^{-1}$ were significantly enhanced compared with those of ST. The peak at 924 $cm^{-1}$ was enhanced because the characteristic peak of acetonitrile (924 $cm^{-1}$) coincided with the characteristic peak of argininamide (915 $cm^{-1}$). However, the characteristic

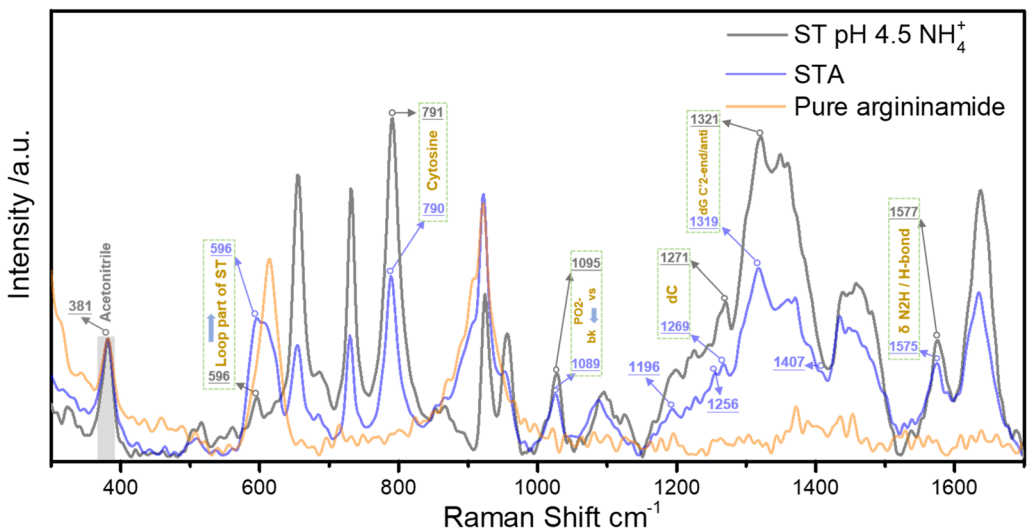


Fig. 4 SERS spectra of ST in the ammonium acetate buffer solution (pH = 4.5; 500 mM), pure argininamide, and STA (1 : 40).

peak intensity of the loop region belonging to ST at 596 $cm^{-1}$ increased significantly. According to the surface selection rules, after incubation, the loop region of STA was perpendicular to the surface of silver nanoparticles in the "hot spot" to enhance the SERS signal. This observation provides evidence for bond cooperation between argininamide and the loop region of ST. In addition, the peak positions of the STA complex at 1271 $cm^{-1}$ (dC) and 1321 $cm^{-1}$(dG C′2*endo*/*anti*) shifted to 1269 and 1319 $cm^{-1}$, which may be due to the formation of hydrogen bonds between argininamide and DNA bases (C, G). At the same time, the band at 1575 $cm^{-1}$ (δN2H) shifted to 1577 $cm^{-1}$, which further confirmed the noncovalent bond (hydrogen bond) between argininamide and ST. The 1360 $cm^{-1}$ (dG $\nu$(C–N) $\delta$(C8–H)) and 1095 $cm^{-1}$ (*vs.* $PO_2^-$) markers moved to 1373 $cm^{-1}$ and 1089 $cm^{-1}$ (bk [$PO_2^-$], *vs.* $PO_2^-$), respectively, indicating that the formation of STA complexes changes the rigid structure. The above experimental results indicated that the current method can detect noncovalent bond interactions (hydrogen bonds) between DNA hairpins and argininamide *via* changes in the SERS characteristic peak of hydrogen bonds and bases and identify the DNA–ligand interaction without labeling.

To further verify the feasibility of the method, we demonstrated the interaction between AP1 and its argininamide ligand by SERS combined with molecular dynamics simulations. AP1 is a variant of the ST sequence. In the inset of Fig. 5(A), it can be observed that the main difference between ST and AP1 is the different order of A, C, T, and G bases in the "stem"; it is clear that the waveforms of the two kinds of DNA (STA and APA) are similar (red and blue lines). Owing to the different coordination sites between argininamide and DNA hairpins, the SERS fingerprint peak-to-peak positions shifted at the two intervals of 1200–1250 $cm^{-1}$ and 1340–1380 $cm^{-1}$. The main difference was that the APA complex showed a strong peak at 1375 $cm^{-1}$ (assigned to dG C2′-*endo*/*syn*). The results revealed that the current method can detect the fingerprint peak of the DNA–ligand samples and identify different variant DNA–ligand samples of the same sequence with good sensitivity.

In Fig. 5SB (ESI†), a positive band and a negative band appear in the CD spectra near 283 nm and 252 nm, respectively, indicating that APA still maintains the DNA hairpin configuration. For example, the waveforms and peak positions of AP1 and APA were similar, and the fingerprint peaks changed in the 1200–1350 $cm^{-1}$ interval (Fig. 5), indicating that the functional groups do not change significantly after the coordination of small molecules. Thus, the current method could determine the range of SERS fingerprint bands corresponding to DNA before and after binding with ligand and also indicated the existence of noncovalent bonds (hydrogen bonds) between argininamide and AP1. We try to precisely predict the interaction between DNA molecules and ligands by theoretical calculations combined with the experimental research. First, we selected the classical ST sequence as the crystal structure of this sequence (PDB ID: 1DB6) has been resolved by NMR and its interaction with argininamide has been characterized.[35] The 100 ns molecular dynamics simulations were performed on the structure of the STA complex and hydrogen bond interactions during simulation times were analyzed. The simulation results suggest that the hydrogen bond interactions between 7A, 8C, 11G, 12T, 14G and 16C of STA were established during the complexation (Fig. 5B and C), which is consistent with the results of its NMR study, indicating the accuracy of the theoretical prediction. We designed and used SERS without labels to detect interaction between ST sequence variant AP1 and argininamide. The 8C and 9G bases of argininamide and AP1 were predicted to be bonded *via* hydrogen bonds through theoretical calculations (Fig. 5B and C). Moreover, RMSD showed that the stability of the rigid DNA is improved after binding of the ligands in STA and APA complexes (Fig. S2, ESI†). The SERS spectra of APA obtained by the current method showed that the characteristic signs of C, $C^+$ and $C{\cdot}C^+$ protonation appeared at 1188, 1205, 1218 and 1407 $cm^{-1}$. In addition, 1244 $cm^{-1}$ (assigned to dG $\delta$NH(N2)), 1270 $cm^{-1}$ (assigned to dC), and 1349 $cm^{-1}$ (assigned to $\nu$(C–N) $\delta$(C8–H)) migrated to 1242, 1268 and 1361 $cm^{-1}$ (assigned to dG C2′-*endo*/*syn*), respectively, and the results showed that argininamide was

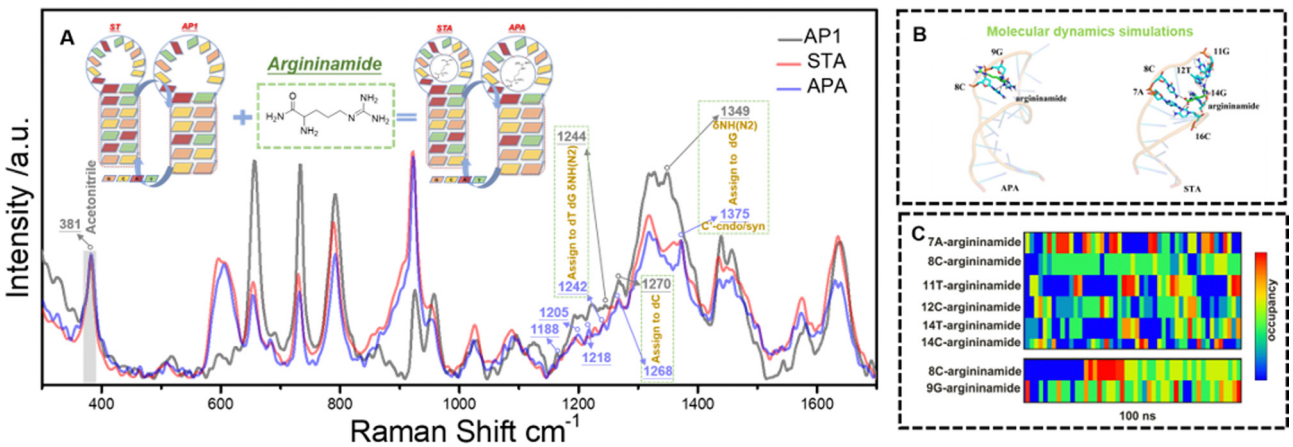


Fig. 5 (A) SERS spectra of AP1, APA, and STA. Inset: Schematic diagram of DNA hairpins (ST and AP1) and argininamide coordination. (B) labeled plots of hydrogen bond interactions predicted by molecular dynamics simulations for STA and APA. (C) the hydrogen bond changes during the molecular dynamics simulations.

 

coordinated with the C and G bases of AP1 by hydrogen bonds, modifying the rigid structure of DNA. The above SERS analysis conclusion was consistent with the molecular dynamics simulation prediction. The results indicated that the current method could predict the binding sites and modes of interaction between DNA and ligands by detecting changes in the hydrogen bonds and SERS characteristic peaks of bases.

## Conclusions

In the present study, a method was developed in which the interaction between DNA and small molecule ligands could be detected without labeling using SERS combined with molecular dynamics simulation. The introduction of the calcium ion aggregator and acetonitrile internal standard significantly improved the ''hot spot'' of traditional silver nanoparticle formation. The current methods can detect changes in the DNA–ligand structure and obtain DNA–ligand interaction signals. SERS was used for the first time to trace changes in the DNA structure caused by the interaction between argininamide and DNA hairpins. Our method can detect the noncovalent bond interaction of DNA–ligands, which was consistent with the predicted results of the molecular dynamics simulations. This new method has good accuracy, sensitivity, and reproducibility and can be used as a general strategy for studying the interaction between DNA and its ligands.

## Author contributions

Yunpeng Wang: conceptualization, data curation, formal analysis, validation, review, editing, writing – review and editing. Na Shi: methodology, formal analysis, data curation. Yingying He: visualization, investigation, data curation, software, writing – original draft. Yang Li: conceptualization, resources, supervision, writing – review and editing. Qingchuan Zheng: conceptualization, resources, supervision, writing – review and editing.

## Conflicts of interest

There are no conflicts to declare.

## Acknowledgements

This work was supported by the Introduce high-level talent incentive project (No.: 0103-31021200052) and HMU Marshal Initiative Funding (No.: HMUMIF-21012); National Natural Science Foundation of China (No.: 82202648).

## Notes and references

1 S. R. Paludan, L. S. Reinert and V. Hornung, *Nat. Rev. Immunol.*, 2019, **19**, 141–153.
2 J. Carvalho, A. Paiva, M. P. Cabral Campello, A. Paulo, J.-L. Mergny, G. F. Salgado, J. A. Queiroz and C. Cruz, *Sci. Rep.*, 2019, **9**, 7945.
3 G. T. Lountos, X. Z. Zhao, E. Kiselev, J. E. Tropea, D. Needle, Y. Pommier, T. R. Burke, Jr. and D. S. Waugh, *Nucleic Acids Res.*, 2019, **47**, 10134–10150.
4 C. F. Landes, Y. Zeng, H.-W. Liu, K. Musier-Forsyth and P. F. Barbara, *J. Am. Chem. Soc.*, 2007, **129**, 10181–10188.
5 B. Berkhout, R. H. Silverman and K.-T. Jeang, *Cell*, 1989, **59**, 273–282.
6 L. Liu, L. Stepanian, D. N. Dubins and T. V. Chalikian, *J. Phys. Chem. B*, 2018, **122**, 7647–7653.
7 X. Guo, Z. Liu, S. Liu, C. M. Bentzley and M. F. Bruist, *Anal. Chem.*, 2006, **78**, 7259–7266.
8 B. J. Calnan, B. Tidor, S. Biancalana, D. Hudson and A. D. Frankel, *Science*, 1991, **252**, 1167–1171.
9 M. Krafcikova, S. Dzatko, C. Caron, A. Granzhan, R. Fiala, T. Loja, M.-P. Teulade-Fichou, T. Fessl, R. Hänsel-Hertsch, J.-L. Mergny, S. Foldynova-Trantirkova and L. Trantirek, *J. Am. Chem. Soc.*, 2019, **141**, 13281–13285.
10 M. Jourdan, A. Granzhan, R. Guillot, P. Dumy and M.-P. Teulade-Fichou, *Nucleic Acids Res.*, 2012, **40**, 5115–5128.
11 F. Wang, C. Wang, Y. Liu, W. Lan, H. Han, R. Wang, S. Huang and C. Cao, *Chem. Commun.*, 2020, **56**, 2099–2102.
12 A. A. Kornyshev, D. J. Lee, A. Wynveen and S. Leikin, *Nucleic Acids Res.*, 2011, **39**, 7289–7299.
13 S. B. Zimmerman and B. H. Pheiffer, *Proc. Natl. Acad. Sci. U. S. A.*, 1979, **76**, 2703–2707.
14 S. You, H.-G. Lee, K. Kim and J. Yoo, *J. Chem. Theory Comput.*, 2020, **16**, 4006–4013.
15 C. L. Manzanares-Palenzuela, A. M. Pourrahimi, J. Gonzalez-Julian, Z. Sofer, M. Pykal, M. Otyepka and M. Pumera, *Chem. Sci.*, 2019, **10**, 10010–10017.
16 R. Galindo-Murillo and T. E. Cheatham, III, *Nucleic Acids Res.*, 2021, **49**, 3735–3747.
17 J. Dash, P. S. Shirude, S.-T. D. Hsu and S. Balasubramanian, *J. Am. Chem. Soc.*, 2008, **130**, 15950–15956.
18 S. S. Tartakoff, J. M. Finan, E. J. Curtis, H. M. Anchukaitis, D. J. Couture and S. Glazier, *Org. Biomol. Chem.*, 2019, **17**, 1992–1998.
19 Z. Asadi, Z. Mandegani, M. Asadi, A. H. Pakiari, M. Salarhaji, M. Manassir, H. R. Karbalaei-Heidari, B. Rastegari and M. Sedaghat, *Spectrochim. Acta, Part A*, 2019, **206**, 278–294.
20 S. Kaneyoshi, T. Zou, S. Ozaki, R. Takeuchi, A. Udou, T. Nakahara, K. Fujimoto, S. Fujii, S. Sato and S. Takenaka, *Chem. – Eur. J.*, 2020, **26**, 139–142.
21 M. Perenon, H. Bonnet, T. Lavergne, J. Dejeu and E. Defrancq, *Phys. Chem. Chem. Phys.*, 2020, **22**, 4158–4164.
22 K. Duskova, P. Lejault, É. Benchimol, R. Guillot, S. Britton, A. Granzhan and D. Monchaud, *J. Am. Chem. Soc.*, 2020, **142**, 424–435.
23 L.-J. Xu, Z.-C. Lei, J. Li, C. Zong, C. J. Yang and B. Ren, *J. Am. Chem. Soc.*, 2015, **137**, 5149–5154.
24 S. Yang, X. Dai, B. B. Stogin and T.-S. Wong, *Proc. Natl. Acad. Sci. U. S. A.*, 2016, **113**, 268–273.
25 Y. C. Cao, R. Jin and C. A. Mirkin, *Science*, 2002, **297**, 1536–1540.
26 S. E. J. Bell and N. M. S. Sirimuthu, *J. Am. Chem. Soc.*, 2006, **128**, 15580–15581.

27 E. Prado, N. Daugey, S. Plumet, L. Servant and S. Lecomte, *Chem. Commun.*, 2011, **47**, 7425–7427.
28 E. Papadopoulou and S. E. J. Bell, *Chem. – Eur. J.*, 2012, **18**, 5394–5400.
29 C. Zong, M. Xu, L.-J. Xu, T. Wei, X. Ma, X.-S. Zheng, R. Hu and B. Ren, *Chem. Rev.*, 2018, **118**, 4946–4980.
30 C. Wei, G. Jia, J. Yuan, Z. Feng and C. Li, *Biochemistry*, 2006, **45**, 6681–6691.
31 Z. Jahnz-Wechmann, J. Lisowiec-Wachnicka, G. Framski, J. Kosman, J. Boryski and A. Pasternak, *Bioorg. Chem.*, 2017, **71**, 294–298.
32 P. C. Lee and D. Meisel, *J. Phys. Chem.*, 1982, **86** 3391–3395.
33 S. Ghosh, S. Mallick, U. Das, A. Verma, U. Pal, S. Chatterjee, A. Nandy, K. D. Saha, N. C. Maiti, B. Baishya, G. Suresh Kumar and W. H. Gmeiner, *BBA, Biochim. Biophys. Acta, Gen. Subj.*, 2018, **1862**, 485–494.
34 J. Kypr, I. Kejnovská, D. Renčiuk and M. Vorlíčková, *Nucleic Acids Res.*, 2009, **37**, 1713–1725.
35 S. A. Robertson, K. Harada, A. D. Frankel and D. E. Wemmer, *Biochemistry*, 2000, **39**, 946–954.
36 *D. Studio*, Accelrys, San Diego, CA, 2011.
37 D. Case, R. Betz, D. S. Cerutti, T. Cheatham, T. Darden, R. Duke, T. J. Giese, H. Gohlke, A. Götz, N. Homeyer, S. Izadi, P. Janowski, J. Kaus, A. Kovalenko, T.-S. Lee, S. LeGrand, P. Li, C. Lin, T. Luchko and P. A. Kollman, *Amber 2016*, *University of California*, *San Francisco*, 2016.
38 F. Wang, W. Sun, C. Xia and Y. Wang, *J. Biol. Inorg. Chem.*, 2017, **22**, 987–998.
39 G. Scuseria, M. Robb, J. Cheeseman, G. Scalmani, V. Barone, B. Mennucci, G. Petersson, H. Nakatsuji, M. Caricato and X. Li, Wallingford, CT, 2009.
40 C. I. Bayly, P. Cieplak, W. Cornell and P. A. Kollman, *J. Phys. Chem.*, 1993, **97**, 10269–10280.
41 J. Wang, W. Wang, P. A. Kollman and D. A. Case, *J. Mol. Graphics Modell.*, 2006, **25**, 247–260.
42 J. A. Maier, C. Martinez, K. Kasavajhala, L. Wickstrom, K. E. Hauser and C. Simmerling, *J. Chem. Theory Comput.*, 2015, **11**, 3696–3713.
43 J. Wang, R. M. Wolf, J. W. Caldwell, P. A. Kollman and D. A. Case, *J. Comput. Chem.*, 2004, **25**, 1157–1174.
44 S. Yoo and S. S. Xantheas, *J. Chem. Phys.*, 2011, **134**, 121105.
45 T. Darden, D. York and L. Pedersen, *J. Chem. Phys.*, 1993, **98**, 10089–10092.
46 V. Krautler, W. F. Van Gunsteren and P. H. Hunenberger, *J. Comput. Chem.*, 2001, **22**, 501–508.
47 D. K. Bhui, H. Bar, P. Sarkar, G. P. Sahoo, S. P. De and A. Misra, *J. Mol. Liq.*, 2009, **145**, 33–37.
48 X. Gao, J. P. Davies and M. J. Weaver, *J. Phys. Chem.*, 1990, **94**, 6858–6864.
49 Y. Li, X. Han, S. Zhou, Y. Yan, X. Xiang, B. Zhao and X. Guo, *J. Phys. Chem. Lett.*, 2018, **9**, 3245–3252.
50 D. Li, Z. Zhang, X. Wang, Y. Wang, X. Gao and Y. Li, *Biosens. Bioelectron.*, 2022, **200**, 113907.
51 N. Yang, Y. Wang, X. Wang, F. Zhang, Y. Xiao, B. Yan, T. Zhang, X. Liu and Y. Li, *J. Phys. Chem. Lett.*, 2022, **13**, 6208–6214.
52 A. C. Garcia, M. Vavrusova and L. H. Skibsted, *Food Res. Int.*, 2018, **107**, 195–205.

 